# Gamma Ray Emission from Radioactive Isobars

Vanessa Kwong

January 8, 2025

**Abstract**

*We study beta and positron decay, along wih electron capture as forms of electrical signals indicating various gamma ray and x-ray emission from $^{57}Co$, $^{137}Cs$, $^{54}Mn$, and $^{22}Na$. Analyzing these spectra through characterization of peaks referencing to $\beta$-decay of $^{60}Co$ and Compton edge behavior, we conclude that $^{137}Cs$ follows $\beta$ decay with the emission 0f a 0.7996±0.0935 MeV between its two energy levels, and $^{22}Na$ follows positron decay with emission of a gamma ray at 0.638±0.2808 MeV indicating the loss of a proton. $^{57}Co$ and $^{54}Mn$ follow electron capture, both with four energy states. $^{57}Co$ emitted at 0.7990±0.0716 MeV, 1.4009±0.08008, 1.5877±0.0714 MeV, and 1.7362±0.0826, while $^{54}Mn$ emitted at 0.8202±0.0336, 1.4365±0.0572, 1.5586±0.0478, and 1.628±0.03947. Furthermore, we illustrate the decay scheme of the measured radioactive isobars, where each peak from energy spectra are represented through gamma ray emission from decay through the energy levels to the daughter nucleus.*

## I Introduction

Three types of decay—beta ($\beta$) decay, positron decay, and electron capture—are studied through collection of gamma-ray energy spectra of five different radioactive materials. Among tested materials are $^{57}$Co, $^{137}$Cs, $^{54}$Mn, $^{22}$Na and $^{60}$Co, which also acts as a calibrating sample.

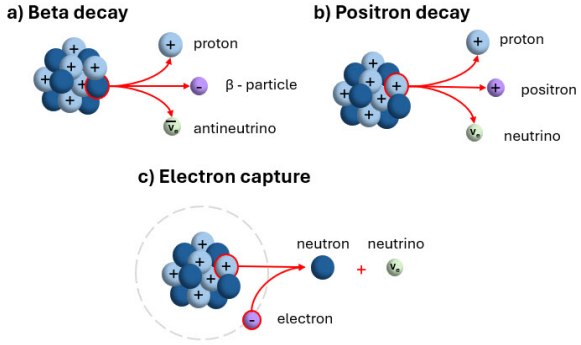


**Figure 1:** Interactions within three forms of decay from parent nuclide, illustrated.

### I.I Beta Decay

During $\beta$ decay (Figure 1a), a neutron ($n$), a neutrally charged particle, splits into a positively charged proton ($p$) and a negatively charged electron ($e^-$), also known as a $\beta^-$ particle, emitting an antineutrino $\bar{\nu_e}$ in the process. [1] This is modeled by:

$$n \rightarrow p + e^- + \bar{\nu_e} \tag{1}$$

The parent nuclide becomes a lesser mass daughter nucleus, where the exothermic conversion of mass to thermal energy released can be accounted for through the following formula for decay energy:

$$E = M_a(Z, A) - M_a(Z + 1, A) \tag{2}$$

where $M_a$ is atomic mass, $Z$ is the number of protons, and $A$ is the total number of protons and neutrons in the nucleus combined. $(Z+1, A)$ gives the state where the nucleus charge is changed through a $\beta^-$ particle emission. [2]

Using $E = mc^2$, we equate the difference in mass, $m = \Delta M$, reduced from $\beta$-decay to the sum ($E = E_\gamma$) of neutrino energy, gamma ray energy, and the emitted electron's kinetic energy. [2]Therefore, we derive

$$\Delta M = \frac{h}{\lambda c} \tag{3}$$

using $E_\gamma = \frac{hc}{\lambda}$. The daughter nucleus decays to ground state afterwards.

### I.II Positron Decay

A positron is a positively charged particle with identical mass to an electron, otherwise referred to its antiparticle. Positron decay (Figure 1b) converts a proton from the parent nucleus to three

particles: a neutron, a positron, and a neutrino $\nu_e$. This is modeled by

$$p \rightarrow n + e^+ + \nu_e \tag{4}$$

Gamma rays are emitted from this process from positrons encountering electrons and colliding, releasing opposite energies, together equal to the same amount as totaled gamma-ray energy. [2] This collision is described by

$$\sum E_\gamma = (M_{e^+} + M_{e^-})c^2) \tag{5}$$

### I.III Electron Capture

Lastly, electron capture (Figure 1c) is described by the K capture process:

$$p + e^- \rightarrow n + \nu_e \tag{6}$$

A proton in the nucleus absorbs an electron, producing a neutron and a neutrino, and leaving a positively charged hole in the original electron's position. A gamma ray is produced since an electron is taken from the innermost K shell, and another higher-energy electron replaces the hole as a result of the missing negative charge. [2]

### I.IV Motivation

When measuring gamma ray emission and observing the spectra giving the collected signals in the form of counts over 8192 energy channels, we can successfully extract properties of the three aforementioned types of decay for the different isobars.We aim to identify these decay schemes based on energy spectra peak characterization and Compton edge behavior.

## II Experimental Procedure

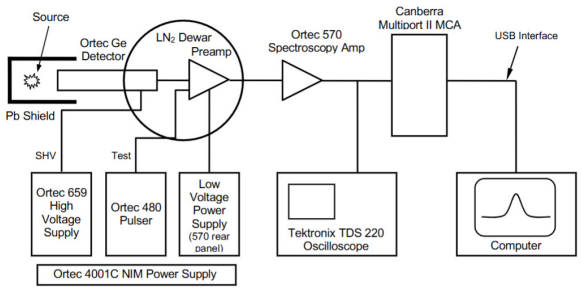


**Figure 2:** Gamma ray spectroscopy setup for emission collection by multichannel GM counter [2]

### II.I Resolution from detectors

For each gamma ray emission measurement, the radioactive material is contained in a lead-shielded box. We use a lithium-drifted germanium (Ge(Li)) detector for its high resolution energy measurements of the tested material, trading off for lower efficiency when compared to sodium iodide crystal scintillation NaI(Tl) detectors. On the other hand, NaI(Tl) detectors have a higher efficiency and lower energy resolution. This often overlooks many other energy levels of interest for gamma ray spectroscopy from giving such broad peaks, making it less optimal for our case.

### II.II Apparatus

The nuclear instrumentation module (NIM) bin power supply consists of a high and low voltage power supply along with a pulser, which will be serve as a standard voltage pulse shown alongside gamma ray data in each spectra.

The energy picked up by the detector is transformed to a voltage signal through the preamplifier in the setup shown in Figure 1. An oscilloscope is used to visualize this amplified signal, and a pulse height analyzer (PHA) sorts the incoming voltage pulses to 8192 channels, each with a different voltage level. Over a span of 600 seconds, data is collected, with signals collecting counts by the multichannel analyzer (MCA) in each channel, eventually creating a large spectra.

### II.III Calibration with $^{60}$Co

A spectra of $^{60}$Co (Figure 3) is first taken to calibrate the system, where its two clearly defined peaks are fitted linearly for channel number to signal voltage (Figure 4). Fitting the two prominent peaks of $^{60}$Co, we find the linear fit equation to be

$$y = 0.22599x - 85.7413 \tag{7}$$

The fitted line passes through both data points and the y-intercept is relatively close to zero, indicating that the energy calibration with NIM bin settings was successful. The spectra for all other materials are taken with this calibration set to determine energy characterization accordingly.

#### II.III.1 Energy Resolution

For each photopeak and pulser peak in the resulting spectra, we note the channel and peak energy through measuring its centroid and full-width-half-maximum (FWHM) when fitting it to a Gaussian function.

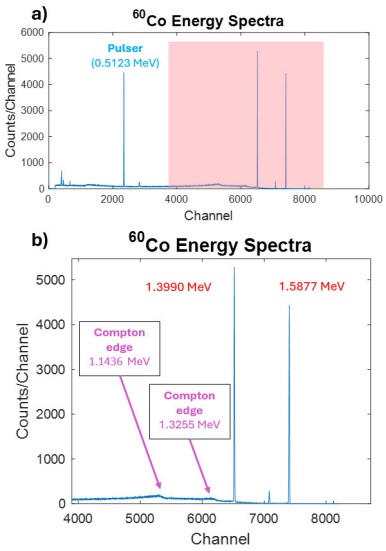


**Figure 3:** Energy spectra of $^{60}$Co; (a) Overall spectra with identified pulser of 0.5123 MeV and two gamma ray peaks within red gamma ray region. (b) Spectra in enlarged gamma ray range showing two Compton edges and prominent peaks of 1.3990 MeV and 1.5877 MeV.

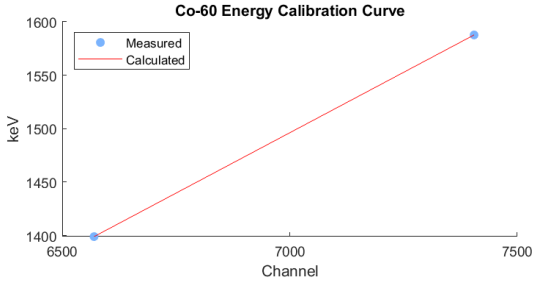


**Figure 4:** Calibration curve from linear fitting for $^{60}$Co peaks, with linear equation (7).

In Figure 3, we can read the value of $R_{elec}$ with the FWHM of the pulser peak, and $R_{det}$ with the FWHM of each following peak. These represent the limit on the energy resolution caused by electronics and the detector, where their relation can be explained by:

$$(R_{det+elect})^2 = (R_{det})^2 + (R_{elect})^2 \tag{8}$$

Analyzing these aspects and recognizing Compton edges, we are then able to identify the decay method for each material. This is first done for the $^{60}$Co sample to quantify the energy resolution of our instrument.

# III Results and Analysis

The decay of the parent nuclei in tested materials consequently gives another material with the proton and neutron ratio equivalent to the daughter nuclei. Identifying the resulting photopeaks, we can classify the materials to one of the three decay schemes.

Peak energies are determined through the collection of counts in the 8192 channels, each indicating a different energy value. Prominent peaks are found at the maximum values of counts, both in the x-ray and gamma ray regions for each spectra. The uncertainty of each peak energy uses the Poisson distribution meant for radioactive decay, since counts in the data are discrete values. We consider the value of uncertainty on both sides of the mean on the x-axis, resulting in the final expression:

$$\mu_s \pm \frac{\sigma}{\sqrt{N}} \tag{9}$$

where $\sigma$ is one standard deviation equivalent to $\sqrt{\bar{R}}$, and $N$ is the number of data points. $\bar{R}$ represents the mean count in the Poisson distribution, telling the average number of decays in a given range of time $\Delta t$. [3]

## III.I Energy Spectra

a)

| Energy | Channel | Uncertainty |
|---|---|---|
| 1.399 | 6570 | 0.1856 |
| 1.5877 | 7405 | 0.1478 |

b)

| Energy | Channel | Uncertainty |
|---|---|---|
| 0.7998 | 3668 | 0.0716 |
| 1.4009 | 6519 | 0.08008 |
| 1.5877 | 7405 | 0.0714 |
| 1.7382 | 8119 | 0.0826 |

c)

| Energy | Channel | Uncertainty |
|---|---|---|
| 0.7996 | 3666 | 0.0935 |

d)

| Energy | Channel | Uncertainty |
|---|---|---|
| 0.8202 | 3765 | 0.0336 |
| 1.4365 | 6688 | 0.0572 |
| 1.5586 | 7267 | 0.0478 |
| 1.628 | 7596 | 0.03947 |

e)

| Energy | Channel | Uncertainty |
|---|---|---|
| 0.6383 | 2902 | 0.2808 |
| 1.5586 | 2909 | 0.2183 |

**Figure 5:** Tables of gamma ray energy peaks, each showcasing energy (MeV), channel number, and uncertainty (MeV) for (a) $^{60}$Co, (b)$^{57}$Co, (c)$^{137}$Cs, (d)$^{54}$Mn, and (e)$^{22}$Na

.

With the count collection for $^{60}$Co (Figure 3), we can identify two prominent gamma ray peaks, each with uncertainties listed in the corresponding table (Figure 5a). The parent nuclei of the sample decay and emit a gamma ray of 1.399±0.1856 MeV, then to a lower energy state, emitting a gamma ray of 1.5877±0.1478 MeV to the daughter nuclei. Measured Compton edges are at 1.1436 MeV and 1.3255 MeV (Figure 3), meaning there is Compton scattering of the following gamma rays at 180°.

The spectra for $^{57}$Co (Figure 6) displays four prominent peaks, where their values with uncertainty are as listed in Figure 5b, There are four energy states in the decay process, first emitting a gamma ray of 0.7990±0.0716 MeV, then 1.4009±0.08008, 1.5877±0.0714 MeV, and

1.7362±0.0826 following, to the daughter nuclei. Two Compton edges are visible, at 0.7384 MeV and 0.7793 MeV.

The spectra for $^{137}$Cs (Figure 7) gives a single energy peak at 0.7996±0.0935 MeV (Figure 5c), and a the gamma ray photon scattering at 0.6153 MeV indicated by the Compton edge.

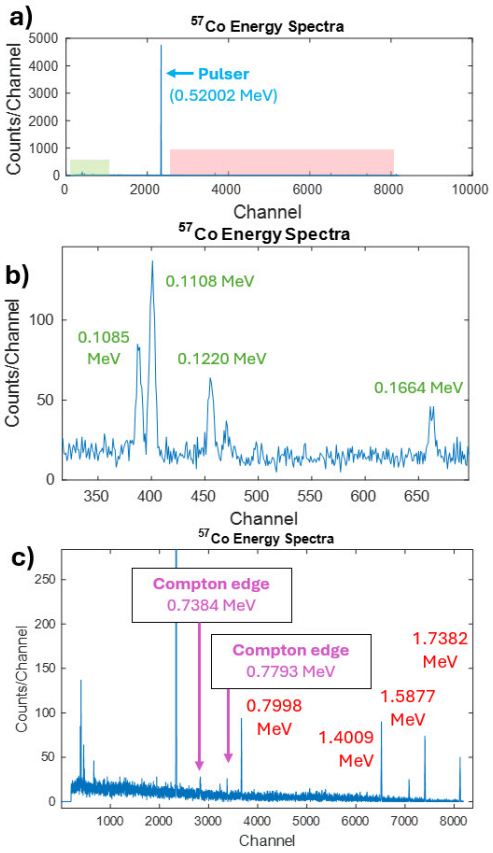


**Figure 6:** Energy spectra of $^{57}$Co; (a) Overall spectra with pulser of 0.52002 MeV, with red region indicating gamma ray range and green indicating x-ray region. (b) Enlarged green region in (a), showing four prominent x-ray peaks. (c) Enlarged red region in (a), showing four prominent gamma ray peaks.

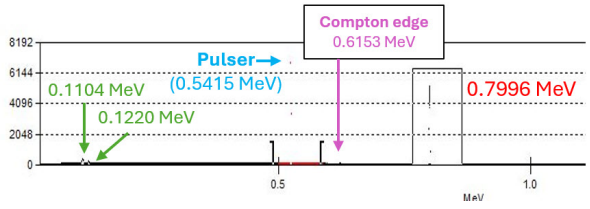


**Figure 7:** Energy spectra of $^{137}$Cs; (a) Enlarged red region in (b), showing one prominent gamma ray peak. (b) Overall spectra with pulser of 0.5415 MeV, with red region indicating gamma ray range and values of x-ray peaks in green.

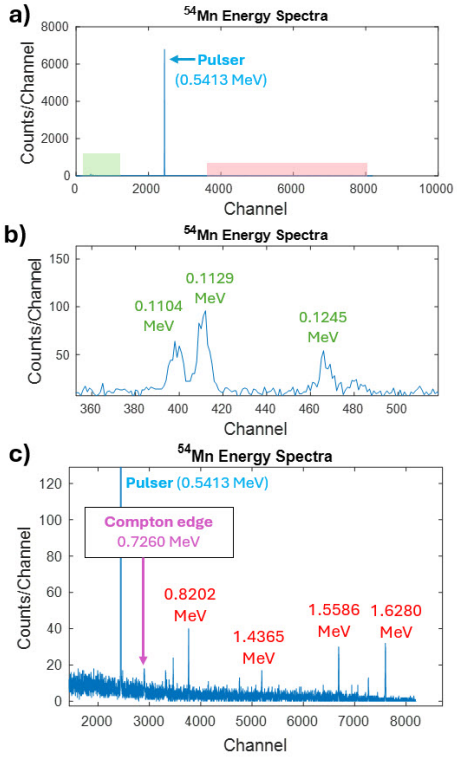


**Figure 8:** Energy spectra of $^{54}$Mn; (a) Overall spectra with pulser of 0.5413 MeV, with red region indicating gamma ray range and green indicating x-ray region. (b) Enlarged green region in (a), showing three prominent x-ray peaks. (c) Enlarged red region in (a), showing four prominent gamma ray peaks.

We evaluate the spectra of $^{54}$Mn (Figure 8) to have four energy peaks, decaying and emitting gamma rays of 0.8202±0.0336, 1.4365±0.0572, 1.5586±0.0478, and 1.628±0.03947 sequentially, as in Figure 5d. A Compton edge is identified, with Compton scattering of a gamma ray encountering an electron at 0.7260 MeV.

Lastly, the decay of $^{22}$Na (Figure 9) emits two prominent gamma rays indicated by the peaks at 0.6383±0.2808 MeV and 1.5586±0.2183 MeV. A Compton edge is identified prior to the pulser peak, at 0.4171 MeV.

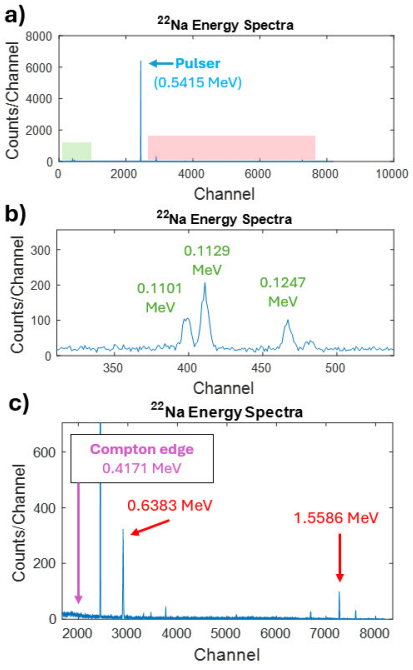


**Figure 9:** Energy spectra of $^{22}$Na; (a) Overall spectra with pulser of 0.5415 MeV, with red region indicating gamma ray range and green indicating x-ray region; (b) Enlarged green region in (a), showing three prominent x-ray peaks; (c) Enlarged red region in (a), showing two prominent gamma ray peaks.

## III.II Nuclear Energy Levels

For each source, we successfully identify the decay scheme. We first classify the decay by identifying the change in number of protons, $Z$. When a proton is gained,

$$(Z, A) \rightarrow (Z + 1, A) \tag{10}$$

whereas the loss of a proton can be modeled by

$$(Z, A) \rightarrow (Z - 1, A) \tag{11}$$

The only decay scheme examined with the gain of a proton is $\beta$ decay, meaning we can conclude materials that go though the process in Eq. 10 to follow $\beta$ decay. [2] When a proton is lost, an emission of a 0.511 MeV gamma ray would indicate that a positron is emitted and the scheme follows positron decay. Therefore, if a proton is lost and the 0.511 MeV gamma ray emission is absent, the material decays through electron capture. [2]

We refer to results from a chemical analysis [2] of daughter nuclei, providing the following:

$$^{60}\text{Co} \rightarrow ^{60}\text{ Ni} \tag{12}$$

$$^{57}\text{Co} \rightarrow ^{57}\text{ Fe} \tag{13}$$

$$^{137}\text{Cs} \rightarrow ^{137}\text{ Ba} \tag{14}$$

$$^{54}\text{Mn} \rightarrow ^{54}\text{ Cr} \tag{15}$$

$$^{22}\text{Na} \rightarrow ^{22}\text{ Ne} \tag{16}$$

### III.II.1 $\beta$-Decay Samples

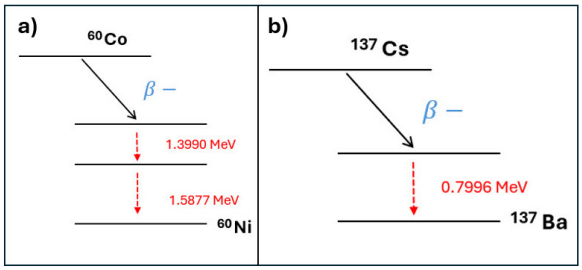


**Figure 10:** Beta decay scheme and nuclear energy level diagrams of $^{60}$Co and $^{137}$Cs, with energy of emitted gamma rays labeled in red ; (a) Decay scheme of $^{60}$Co with two emitted gamma rays to reach daughter nucleus of $^{60}$Ni; (b) Decay scheme of $^{137}$Cs with one emitted gamma ray to reach daughter nucleus of $^{137}$Ba.

$^{60}$Co, the calibration sample, undergoes $\beta$ decay. Referencing to a periodic table, standard Ni has one more proton than Co. Taking into account the atomic numbers and identical masses of both, we can conclude a proton is gained and neutrons are lost, where

$$^{60}\text{Co} = 27p + 32n \tag{17}$$

$$^{60}\text{Ni} = 28p + 30n \tag{18}$$

This is a characteristic of $\beta$ decay, in reference to Eq. 10 and Eq. 2, and we can illustrate the decay in Figure 9a. Here, the energy is distributed to the the neutrino, emitted electron, and gamma ray separately.

Likewise, $^{137}$Cs also undergoes beta decay with the same identification method, where

$$^{137}\text{Cs} = 55p + 82n \tag{19}$$

$$^{137}\text{Ba} = 56p + 81n \tag{20}$$

However, we can illustrate this decay scheme in Figure 9b, where the difference in mass between the two nuclei are the total energies of the emitted and conversion electron with x-ray energy. [2]

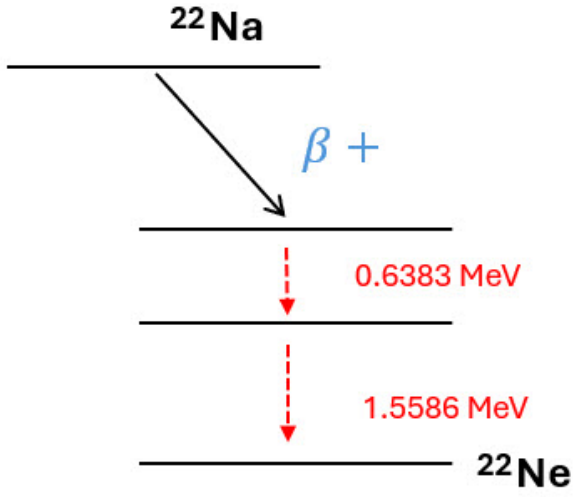


**Figure 11:** Positron decay scheme and nuclear energy level diagram of $^{22}$Na, with energy of emitted gamma rays labeled in red; Two gamma rays are emitted to reach daughter nucleus of $^{22}$Ne.

### III.II.2 Positron Decay Sample

Characterized by the loss of a proton, positron decay also includes the emission of a gamma ray where $\gamma$ =0.511 MeV. [2] This is observed in $^{22}$Na, where the relation in Eq. 16 implies

$$^{22}\text{Na} = 11p + 11n \tag{21}$$

$$^{22}\text{Ne} = 10p + 12n \tag{22}$$

with less protons and more neutrons after the decay. In addition, we refer to the spectra of $^{22}$Na (Figure 8), confirming a gamma ray signal from positron emission. There is a prominent peak at approximately 0.6383 MeV, relatively close to the theoretically expected 0.511 MeV peak. We confirm the decay scheme and nuclear energy level diagram in Figure 11.

### III.II.3 Electron Capture Decay Samples

Two samples—$^{57}$Co and $^{54}$Mn—unclassified as either $\beta$-decay or positron decay are confirmed to follow the electron capture decay scheme. Referring, again, to proton count and atomic mass, we see

$$^{57}\text{Co} = 27p + 30n \tag{23}$$

$$^{57}\text{Fe} = 26p + 31n \tag{24}$$

for $^{57}$Co and

$$^{54}\text{Mn} = 25p + 29n \tag{25}$$

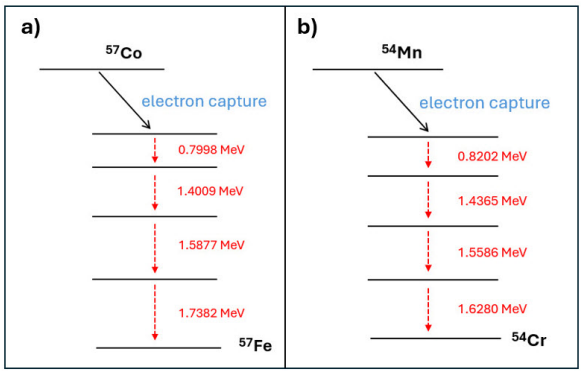


**Figure 12:** Electron capture decay scheme and nuclear energy level diagrams of $^{57}$Co and $^{54}$Mn, with energy of emitted gamma rays labeled in red ; (a) Decay scheme of $^{57}$Co with two emitted gamma rays to reach daughter nucleus of $^{57}Fe$; (b) Decay scheme of $^{54}$Mn with one emitted gamma ray to reach daughter nucleus of $^{54}$Cr.

$$^{54}\text{Cr} = 24p + 30n \tag{26}$$

for $^{54}$Mn.

Neither spectra have a notable peak at around 0.511 MeV despite the loss of a proton, meaning their can only be classified as electron capture. With this, we illustrate the decay scheme of $^{57}$Co (Figure 10a) and $^{54}$Mn (Figure 10b).

## IV Conclusion

We have successfully characterized the gamma ray energy spectra of radioactive samples with reference to a standard $^{60}$Co spectra and conclude their decay routes. Beta decay is seen in $^{137}$Cs. Positron decay is seen in $^{22}$Na. Electron capture is seen in $^{57}$Co and $^{54}$Mn. These results are consistent with literature results [4] [5] [6] [7]. Beta decay involves the loss of a neutron and is characterized by–, whereas positron decay includes the loss of a proton–. Electron capture involves the absorbance of an electron in the inner shell with a proton to result in an additional neutron, with a neutrino as its byproduct.

Improvements can be made to this study through testing each material for multiple trials, as this would provide higher precision and lower uncertainties for each photopeak characterization. Likewise, precision can also be improved through obtaining each data set for a longer span of time. With a collection time of over 600 seconds, less prominent peaks in the spectra are likely to emerge and become more visible, if unidentified. Drift, such as from environmental differences throughout the day and week of measurement, may also play a role in measurement offsets. This is especially notable for the instrumentation of this experiment as the Ge

detector requires a low temperature, achieved by a liquid nitrogen cool-down to function properly.

For additional applications, we can implement the aforementioned improvements, along with using a multichannel analyzer separating the voltage range into a higher number of channels. This results in an even higher preciseness of measurements.

# References


[1] H. S. Matis, *Beta Decay*. Guide to the Nuclear Wallchart, 2009.

[2] W. P. Beyermann, "Gamma ray emission from radioactive isobars," 2024.

[3] W. P. Beyermann, *Uncertainty and Statistics*.

[4] A. A. Faraj, B. Alotaibi, A. P. Shaik, K. Shamma, I. A. Jammaz, and J. Gerl, "Sodium-22-radiolabeled silica nanoparticles as new radiotracer for biomedical applications: in vivo positron emission tomography imaging, biodistribution, and biocompatibility," *Int J Nanomedicine*, vol. 10, pp. 6293–6302, 2015.

[5] I. W. Goodier, J. L. Makepeace, and L. E. H. Stuart, "The decay scheme of caesium 137," *The International Journal of Applied Radiation and Isotopes*, vol. 26, 1975.

[6] K. Zaerpoor, Y. D. Chan, and D. E. DiGregorio, "Galactic confinement time of iron-group cosmic rays derived from the m54n chronometer," *Physical Review Letters*, vol. 79, pp. 4306–4309, 1997.

[7] J. M. Ferguson, "Co-57 decay scheme," *Nuclear Physics*, vol. 10, pp. 405–411, 1957.